

# Design of energy efficient ice-skating rink using phase change material

Tran Le Vu<sup>1\*</sup>, Sivanand Somasundaram<sup>1</sup>, Swapnil Dubey<sup>1</sup>, Govind Harikumar<sup>1</sup>, Srinivasa Rao Purimitla<sup>1</sup>, Jacques Mouchet<sup>2</sup>

1 Energy Research Institute @ Nanyang Technological University, #06-04, Cleantech One, 1 Cleantech Loop, Singapore 637141

2 Sun-Ice Energy Pte Ltd, 16 Enterprise Rd, Singapore 627699

(\*Corresponding Author: levu.tran@ntu.edu.sg)

## ABSTRACT

Conventional ice-skating rinks require an intensive refrigeration load and continuous use of chiller which results in a substantial energy consumption. Therefore, novel, and sustainable alternatives are required to make more energy efficient ice-skating rinks. In this study, we propose a novel first-of-a-kind PCM (Phase Change Material) based ice skating rink and report the development of computational tool based on CFD (Computational Fluid Dynamics) to study various design aspects of such innovative system. The overall results show the significance of this model in providing a powerful tool to select suitable PCM, test operating parameters such as inlet temperature and flow rate, as well as predict the ice rink performance under different scenarios.

**Keywords:** Ice-skating rinks, CFD, PCM

## NONMENCLATURE

<i>Abbreviations</i>	
CFD	Computational Fluid Dynamics
PCM	Phase Change Material
<i>Symbols</i>	
$\rho$	Density
$c_p$	Specific heat
$T$	Temperature
$q''$	Heat flux vector
$A$	Control surfaces
$V$	Control volumes
$E$	Total energy
$H$	Total enthalpy
$\mathbf{v}$	Velocity vector
$\mathbf{T}$	Viscous stress tensor
$\alpha_i$	Volume fraction of phase $i$
$\mathbf{v}_m$	Phase mixture velocity vector

## 1. INTRODUCTION

Ice rinks are typically used for ice skating and playing winter sports. However, they are also used for exhibitions, contests, and ice shows. An ice-skating rink maintains a frozen body of water on the surface by an indirect cooling system underneath. In conventional design of ice-skating rinks, refrigerated brine solution is pumped through a maze of pipes located underneath the ice sheet to keep it frozen. Deionized water is put down in thin layers freezing on the chilled surface until it is about one inch thick. The use of deionized water allows clear ice to form. This design depends on continuous use of chiller and continuous dependence on power source to run the chiller. Since the ice-skating rinks' operating cost is high due to high cooling loads, novel and sustainable alternatives are required to make more energy efficient ice-skating rinks.

We propose a novel first-of-a-kind PCM (Phase Change Material) based ice skating rink. In this proposed design, the chillers are designed to operate during the day using electricity produced from PV panels. The excess cold energy produced during the day is stored in the PCM (to solidify the PCM from liquid to solid state). The stored cold energy in PCM is intended to be used during evening and nighttime and during rain or cloudy weather periods when there is less or no PV output. Figure 1 illustrates this patented design in which PCM containers are integrated into a conventional ice-skating rink.

For the current novel design, the following research questions were the motivation of the current work. What is the optimal PCM phase change temperature that can be used to store excess cold energy? That is, a PCM having lower phase change temperature may reduce the coefficient of performance (COP) of the chiller and

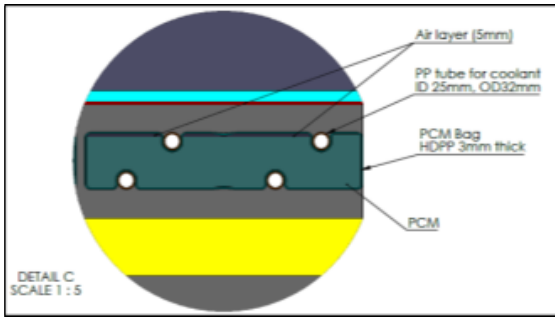


Fig. 1. The patented design of PCM material integrated ice-skating rink

require high energy requirement; whereas a PCM having higher PCM temperature has a lower capability to store excess cold energy. This necessitates an optimal point to be chosen. Secondly, for a given design configuration, what is the charging time which is the conversion of liquid PCM to solid PCM and the discharging time which is the conversion of solid to liquid?

In literature, ice-skating rinks were subjected in a study on different envelop configurations: concrete structure and air-supported membrane structure [1]. Research on improving thermal and humidity condition was conducted by [2] and [3] in both experimental and numerical perspectives. [4] studied heat loads on the ice rink by radiation, condensation, and convection. However, there is no study referring to integrating PCM to the refrigeration system of ice-skating rinks.

Heat transfer throughout the entire system is a crucial engineering process that would influence the charging time needed for storing and releasing thermal energy. Therefore, conjugate heat transfer between

various components of the patented design were considered. Another crucial physics process is the phase change during melting and solidification of the PCM, as well as the occurrence of ice formation on the rink surface. These require a multi-physics simulation approach. Computational fluid dynamics is a numerical modelling tool for heat transfer and fluid flow and was adopted in many previous studies to simulate such processes. In literature, reviews on multi-physics simulations can be referred to [7], whereas ones on computational fluid dynamics simulation studies in phase change materials were conducted in [5], [6].

In this paper, we present the development of a high-fidelity multi-physics numerical simulation model that aims to simulate the physics involved in an innovative ice-skating rink utilized PCM material. STAR-CCM+ was validated for phase change flows in previous study such as in [8]–[12], hence, was adopted for building up such simulation model. The model is then used to identify the appropriate PCM material that facilitates the formation of high-quality ice on the innovative ice-skating rink. Various phase change temperatures of PCM materials are considered to determine the charging and discharge performances. In addition, we studied ice formation processes and reported typical ice surface heat flux at the ice formation layer.

## 2. METHODOLOGY

### 2.1 Geometry

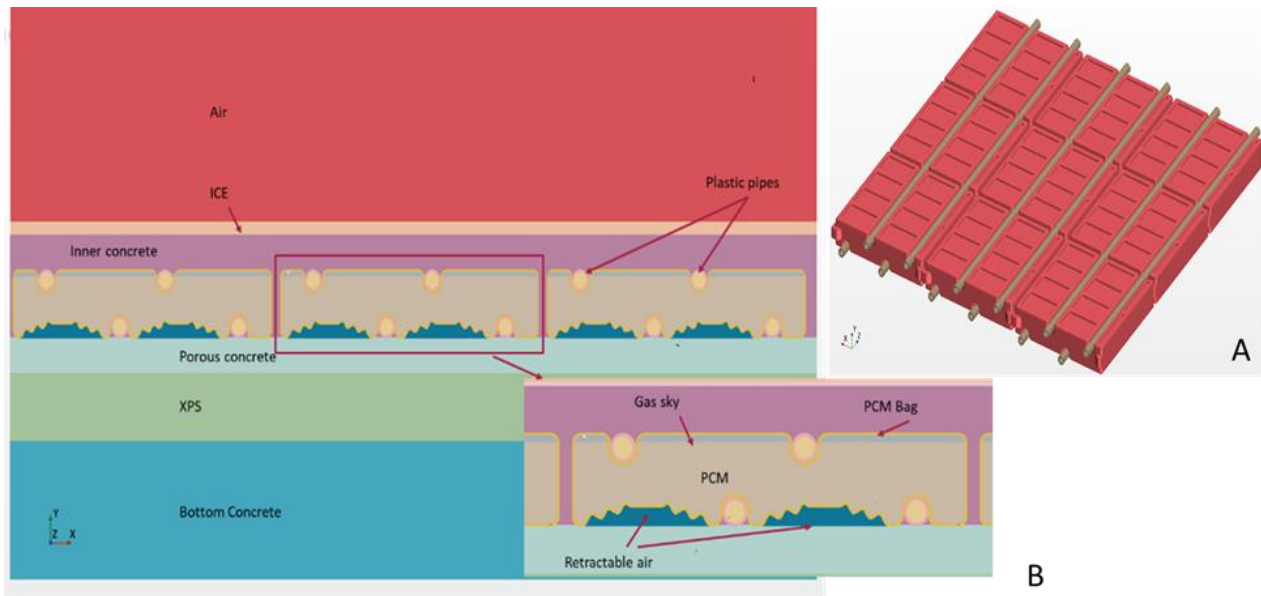


Fig. 2. (A) The PCM containers made of HDPE material will be initially filled with liquid PCM. (B) Sectional view of the computational geometry with indicated various regions of the whole ice-skating rink structure

Figure 2 shows a matrix of three-by-three PCM containers made of High-Density Polyethylene (HDPE) which is the main component of geometry considered in the following numerical study. These containers are initially filled with liquid PCM. Other items can be shown in this figure are plastic pipes which coolant heat transfer fluid (HTF) flows through and exchanges heat with the PCM material.

The sectional view of a full CAD model comprised of various regions representing the whole ice-skating rink structure is also depicted in Figure 2. The lowest layer is the bottom concrete served as the base of the whole structure. Next is an insulation layer made of Extruded Polystyrene Insulation (XPS) material to prevent heat loss from the PCM materials. As mentioned earlier, PCM containers and the coolant flows of HTF piped through plastic pipes can also be shown in the figure. They are enclosed in an Inner Concrete layer and sit above a porous concrete layer. Noticeably, there is a retractable air gap between the porous concrete and PCM containers which allows air to pass through and ensures PCM expansion during the melting and solidification process does not affect the structure. The last two layers sitting on top of the Inner concrete layer are a 25-mm ice layer and a 6-m air domain extended above ice surface.

## 2.2 Governing equations and simulation models

In STAR-CCM+, a specific set of physics models, included in so called continua, is applied to each domain region to solve the physical process involved. Therefore, each region in Figure 2 is associated with a separated continua where physic models, initial and reference values are defined. In general, of all eight regions in the ice rink, there are three typical flows considered.

In the solid regions such as Bottom concrete, Insulation, Porous concrete, Inner concrete, PCM shell, and Coolant pipes, segregated solid energy model was adopted to solve energy equation in these regions. The governing equation for energy transport reads:

$$\frac{d}{dt} \int_V \rho c_p T dV = - \oint_A q'' \cdot dA \quad (1)$$

Where  $\rho$ ,  $c_p$  are density and specific heat properties,  $T$  is temperature,  $q''$  is the heat flux vector,  $A$  and  $V$  are control surfaces and volume.

In fluid regions such as HTF flows, segregated flow solver which solves integral conservation equations of mass and momentum sequentially was selected. SIMPLE algorithm was implemented in the solver for pressure-velocity coupling. Energy transport equation was

handled by the segregated fluid temperature model which the following equation is solved:

$$\frac{d}{dt} \int_V \rho E dV - \oint_A \rho H \mathbf{v} \cdot d\mathbf{A} = - \oint_A q'' \cdot d\mathbf{A} + \oint_A \mathbf{T} \cdot \mathbf{v} d\mathbf{A} \quad (2)$$

Where  $E$  and  $H$  are total energy and enthalpy,  $\mathbf{v}$  is velocity vector, and  $\mathbf{T}$  is the viscous stress tensor. Other assumptions were employed for fluid regions are:

- Constant density flow, and
- Laminar flow

Multiphase model is utilized in the water and PCM regions, where phase change process occurs. There are various options available in STAR-CCM+. In this study, the VOF (volume of fluid) approach is adopted for both the liquid and solid phases. The VOF model postulates that within a control volume, all immiscible fluid phases have a shared velocity, pressure, and temperature. Consequently, the governing equations describing momentum, mass, and energy transport in a single-phase flow are utilized. These equations are computed based on the physical properties of each constituent phase and their respective volume fractions. The conservation equation used for the transport of volume fractions  $\alpha_i$  applies to the liquid zone (where the solid fraction  $\alpha_s = 0$ ) and the mushy zone (where  $0 < \alpha_s < 1$ ):

$$\frac{d}{dt} \int_V \alpha_i dV + \int_A \alpha_i \mathbf{v}_m \cdot d\mathbf{A} = 0 \quad (3)$$

The following functionalities of STAR-CCM+ are incorporated in the VOF model setting:

- Phase transition based on the volume's temperature
- Laminar natural convection within the liquid region
- The presence of a mushroom-shaped region between the solid and liquid phases
- Density that varies with temperature
- The solid fraction's flow cessation criterion, set at 0.99

## 2.3 Mesh generation

There are three meshers options selected to generate the final mesh in STAR-CCM+. First, the surface mesher utilized triangle elements to represent the outer surface of the domain, then polyhedral mesher was used to construct the volume mesh. In solid regions such as

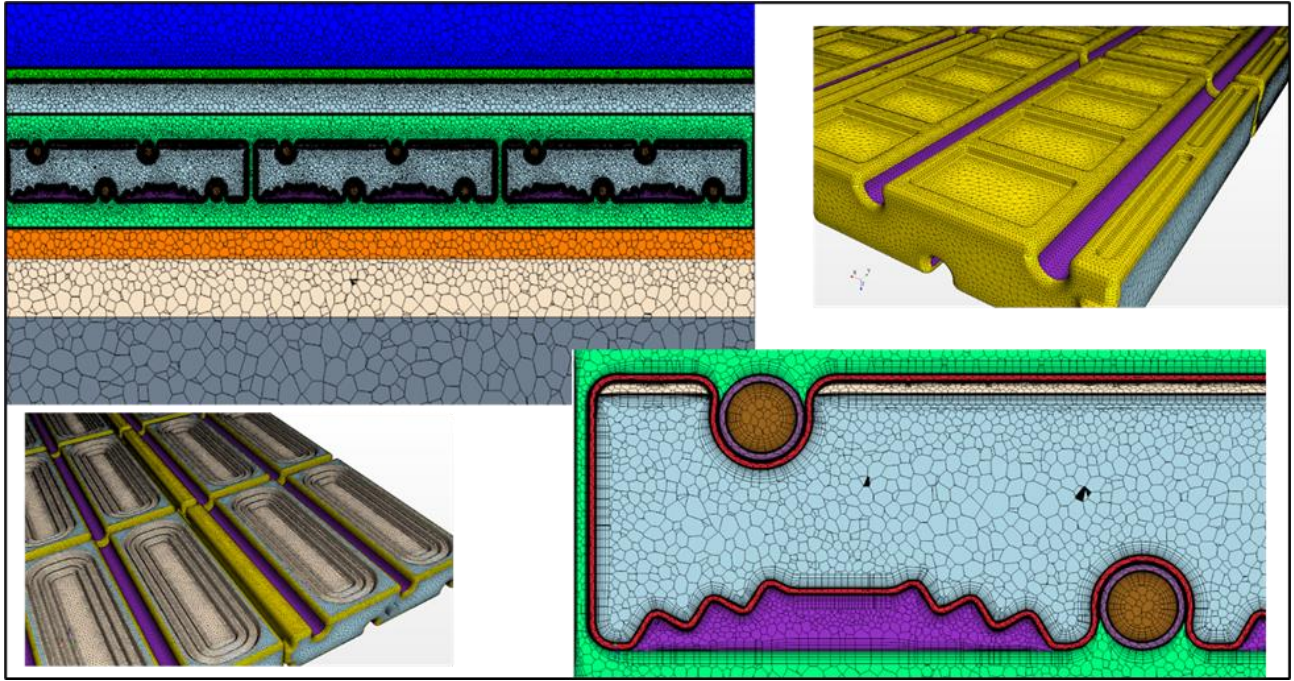


Fig. 3. Sectional view of the mesh

pipes and PCM containers, a thin mesher was used to capture these thin solid material thickness. One of the significant parameters of surface mesher and polyhedral mesher is the base mesh size. Therefore, various mesh sizes were subjected to a mesh sensitivity study in the following section to finalize this parameter. Additionally, five layers of prismatic elements were employed to capture the boundary layer physics near the liquid/fluid surfaces. These prismatic layers were disabled in the mentioned solid regions. The final mesh can be shown in Figure 3.

#### 2.4 Mesh sensitivity study

Before running simulation, a mesh sensitivity study was conducted to evaluate the effects of mesh parameters on the results. Three meshes with varied number of cells are generated as summarized on Table 1.

Table 1: Mesh metrics and results

Case Number	Total mesh cell counts	Solidification time (Hours)	Errors
Mesh 1	704,157	47.33	-4.09%
Mesh 2	1,283,800	49.35	Base
Mesh 3	2,155,221	49.83	+0.97%

Mesh 2 is selected as the base mesh. Mesh 1 has the lowest mesh counts, whereas Mesh 2 and Mesh 3 have 1.8- and 3.1-times greater number of mesh elements, respectively. These meshes are subjected to the same base simulation. Results of solidification time in hours and corresponding relative errors to the base mesh are

recorded in the table. We can see that Mesh 2 and Mesh 3 generate comparable results even though the prior mesh has only half the mesh counts of the later one. Figure 4 further confirms this similarity which compares temporal profiles of solid volume fraction of the PCM during simulations of Mesh 1, Mesh 2, and Mesh 3. It shows that there is a deviation in results between Mesh 2 and Mesh 3, nevertheless, lines of Mesh 2 and Mesh 3 are mostly overlapped.

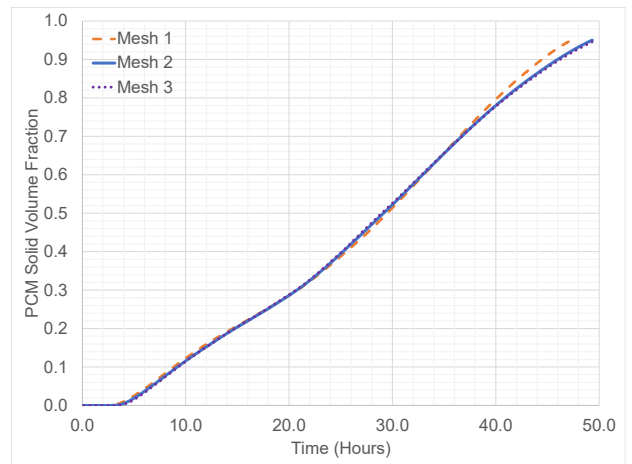


Fig. 4. Mesh sensitivity study result

### 3. RESULTS AND DISCUSSION

#### 3.1 PCM selection

Table 2: PCM candidates' properties

PCM	Latent Heat	Phase change temperature	Solid Density	Liquid Density	Thermal Conductivity	Specific Heat
	kJ/Kg	°C	Kg/m <sup>3</sup>	Kg/m <sup>3</sup>	W/m-K	J/Kg-K
PCM-11	290	-11	1200	1100	0.6	2000
PCM-17	300	-17	1200	1100	0.6	2000
PCM-24	250	-23	1200	1300	0.6	2000

One of advantages of CFD is an ability to test different scenarios of working conditions without conducting costly experiments. The first task of developing this innovative ice-skating rink is to select an appropriate PCM which supports desired operations and with good performances.

We selected three candidate PCM and subjected them to a performance comparison study. Table 2 summarizes their thermal and physical properties. They are under the same category of inorganic PCM; therefore, we could see most properties are shared but the phase change temperature which differs from -11°C to -23°C.

There are two simulations conducted for each PCM. Initial charging simulation assumes the PCM charging process is started from ambient temperature and completed when reaching 95% of solid volume fraction. Heat transfer fluid (HTF) used is Glycol-water solution 50% and the mass flow rate of 0.6 kg/s. To have a fair comparison between the different phase change temperature of the candidate PCM, we assumed the temperature difference between HTF inlet and PCM temperature is the same:  $\Delta T = -8^\circ\text{C}$ . The outlet condition is applied at the exit boundary of HTF which assumes no reverse flow. The bottom surface of the bottom concrete region has a fixed temperature condition  $T_{\text{bot}} = 5^\circ\text{C}$ . This is also a general practice as a heated flow is used to keep this surface warm and prevent overcooling of adjacent structures. Adiabatic wall condition is adopted for all other outer surfaces of the domain, therefore, an ideal condition of thermal isolation with surroundings is assumed for all PCM. The initial temperature of all domains was at  $5^\circ\text{C}$ .

Consequently, the state of the charging simulation is set as the initial condition for discharging simulation. In this stage, the HTF flow is stopped, and a heat flux is applied at the top surface of ice layer region. A typical value of heat load  $135.25 \text{ W/m}^2$  is adopted. The stopping criteria of the simulation is when the temperature of ice at top surface is more than desired temperature of  $-6^\circ\text{C}$ .

Comparison of results of the initial charging simulations is depicted in Figure 5. The charging time of three PCM are also extracted in this figure. Although the PCM-11 has the fastest rate of charging initially, its final

charging time is larger than of the PCM-24. This may be due to the lower latent heat of PCM-24 which lessens the heat required to solidify the PCM. PCM-17 has the largest charging time, 4.4% and 8.5% more than PCM-17 and PCM-11, respectively.

Ice temperature and PCM solid volume fraction during discharging are reported and presented in Figure 6. We could see that the initial temperature of ice region

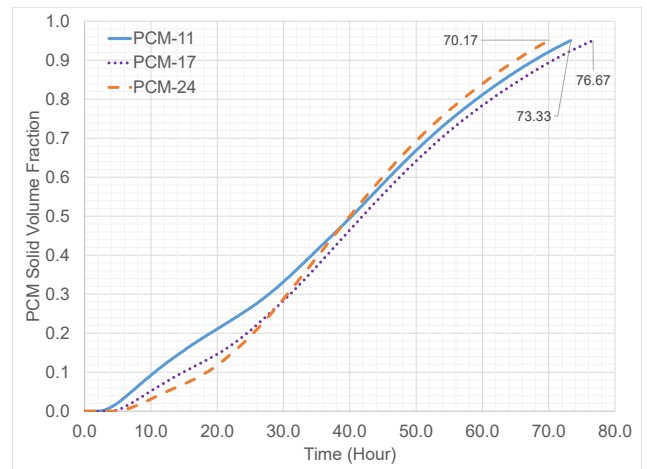


Fig. 5. Comparison of profiles of PCM solid volume fraction during initial charging simulations of three candidate PCM: PCM-11, PCM-17, and PCM-24.

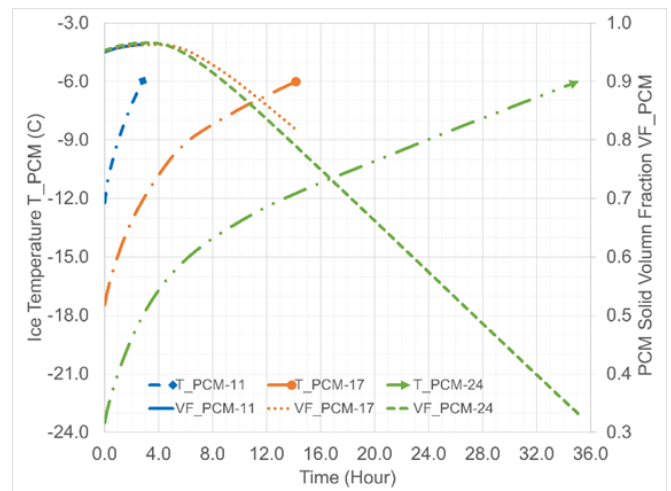


Fig. 6. Discharging simulation results comparison (1) profiles of ice temperature at top surface; and (2) profiles of PCM solid volume fraction of PCM-11, PCM-17, and PCM-24.

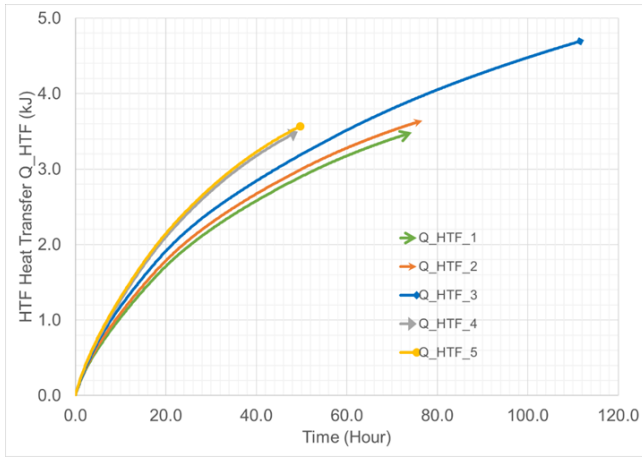


Fig. 7. Profiles of heat transfer energy from HTF during simulations of HTF inlet conditions

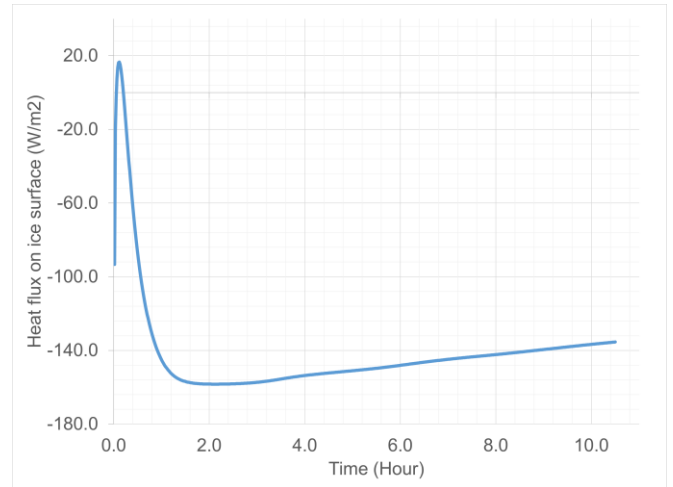


Fig. 8. Heat flux on ice surface fixed at  $-6^{\circ}\text{C}$  with glycol flow on up to 30 mins and then turned off

is quite close to phase change temperature of PCM which resulted from the charging step. Consequently, PCM-11 had a noticeably short discharging time, whereas PCM-24 took an extended period of discharging and exhausted a significant fraction of PCM solid volume (to around 33%). PCM-17 had a balanced discharging performance of around 14 hours discharging time and the change in solid volume fraction was around 81.5%.

The results of this comparison study are summarized in Table 3. Although PCM-17 has 8.5% larger charging time in comparison with the best charging time, its discharging results outperform other PCM as it can sustain the desired ice temperature for more than 12 hours and keep the remained PCM solid volume fraction above 80% for this operation. PCM-24 may require less recharges, nevertheless, significant difference between desired ice temperature and PCM temperature can work only when the heat load from the air side above the ice layer is high enough to maintain the ice temperature between  $-6$  to  $-7^{\circ}\text{C}$ .

### 3.2 HTF inlet condition test simulations

Based on the selected PCM, another set of test cases were analyzed for HTF inlet conditions. The solidification time which is required for the initial liquid PCM to solidify was assessed considering different coolant flow rates and varying inlet temperature. Other operating and boundary conditions are the same as the previous

section. Summary of these test cases is in Table 4. Results of solidification time are also consolidated in this table.

Figure 7 reports the total heat transfer from HTF flows over time, we can see Case 4 and Case 5 which have the lower HTF inlet temperature resulted in the lowest charging time. There was insignificant difference in the charging performance between these two cases, even though Case 3 has a much larger HTF flow rate. This also can be confirmed when we compare Case 1 and Case 2 results.

Surprisingly, Case 3 has the highest flow rate but the worst charging time in all cases. Examine Figure 7 in terms of rate of increase in total heat transfer energy, in comparison with Case 2 which has a lower flow rate, Case 3 has faster heat extraction but lower PCM solidification time. This indicates an inefficient utilization of cold energy regarding charging PCM containers.

### 3.3 Ice formation and required ice surface heat flux

In this section, a two-stage simulation was conducted to emulate the ice formation process in an actual scenario, where water is poured over the rink after the PCM is solidified and the top concrete layer reaches  $-4^{\circ}\text{C}$ . The initial stage of the simulation focused on allowing the liquid PCM to solidify and monitoring temperature of the top concrete surface. Once this temperature decreases to a minimum of  $-4^{\circ}\text{C}$ , heat transfer was enabled, leading to the formation of ice on

Table 3: PCM comparison results summary

PCM	Initial charge time (hours)	Discharge time (hours)	Remained PCM volume fraction (%)
PCM-11	73.3	3.0	96%
PCM-17	76.7	14.0	81.5%
PCM-24	70.2	35.0	33%

top of the PCM container's concrete layer. The desired surface temperature of the ice layer is approximately  $-6^{\circ}\text{C}$ . It is of interest to see if the ice temperature of  $-6^{\circ}\text{C}$  can be maintained consistently over a prolonged period by the chosen PCM material. Initial simulations indicated that the cooling rate provided by the PCM was high. Hence, a significant heat load from above air layer is required to balance this and maintain the ice temperature at  $-6^{\circ}\text{C}$ . Therefore, the simulation was extended to estimate this heat load for the current design.

In this extended simulation, we applied a fixed ice surface temperature at  $-6^{\circ}\text{C}$  and aimed to estimate the heat load needed to sustain this temperature over a 10-hour period. During this period, there is no HTF flow, and the dominant cooling comes from a solid PCM at low temperatures. The air region in the original model was disregarded as a fixed temperature was applied on the ice layer top surface.

Figure 8 illustrates the varying of heat flux on ice top surface during the simulation. At the 30-minute mark, the required heat flux is  $-87.13\text{ W/m}^2$ . After 10 hours without glycol but with only PCM, the heat flux on the ice surface reaches approximately  $-136.58\text{ W/m}^2$ . Over a 10-hour period of discontinuing glycol flow, an average surface heat flux of  $-146.96\text{ W/m}^2$  is necessary to uphold the ice surface at the target temperature of  $-6^{\circ}\text{C}$ .

#### 4. CONCLUSION

We reported in this paper the development of a CFD model for studying heat transfer process in an ice-skating rink integrated PCM. The overall results show the significance of this model in providing a powerful tool to select suitable PCM, test operating parameters such as inlet temperature and flow rate, as well as predict the ice rink performance under different scenarios.

One limitation of current study is on modeling heat transfer process in the air layer above the ice layer which considered only conduction and convection, even though radiation may be the significantly contributed to the total heat flux to the ice surface. Therefore, enhancements of physical model for air layer are under development and to be discussed in future paper. Additionally, as PCM integrated ice rink is the first of its kind, there is an on-going effort to build up an experimental test bed which models this innovative ice rink. Data from this will prove the effectiveness of this new concept and provide more data for the simulation model validation.

#### ACKNOWLEDGEMENT

This work was funded by a joint collaboration project between Energy Research Institute @ Nanyang Technological University (ERI@N) and Sun-Ice Energy (sun-ice-energy.com) under NTU Reference No. REQ0236468 to establish the model design and simulation of Phase Change Material (PCM) based innovative Ice-Skating Rink for energy saving potential in skating rink operation. Sun-Ice Energy is a Singapore registered company aims to build "The Future of Sustainable Cooling for Positive Energy Buildings". The design used in this paper is protected by patents and utilised to develop the world's first solar cooled ice-skating rink.

#### DECLARATION OF INTEREST STATEMENT

The authors declare that they have no known competing financial interests or personal relationships that could have appeared to influence the work reported in this paper. All authors read and approved the final manuscript.

#### REFERENCE

- [1] W. Lin, X. Liu, S. Li, and T. Zhang, "Investigation on thermal environment and heat transfer characteristics in ice rinks with different envelopes," *Build. Environ.*, vol. 219, p. 109250, Jul. 2022, doi: 10.1016/j.buildenv.2022.109250.
- [2] A. Palmowska and B. Lipska, "Experimental study and numerical prediction of thermal and humidity conditions in the ventilated ice rink arena," *Build. Environ.*, vol. 108, pp. 171–182, Nov. 2016, doi: 10.1016/j.buildenv.2016.08.024.
- [3] A. Palmowska and B. Lipska, "Research on improving thermal and humidity conditions in a ventilated ice rink arena using a validated CFD model," *Int. J. Refrig.*, vol. 86, pp. 373–387, Feb. 2018, doi: 10.1016/j.ijrefrig.2017.11.016.
- [4] A. Daoud, N. Galanis, and O. Bellache, "Calculation of refrigeration loads by convection, radiation and condensation in ice rinks using a transient 3D zonal model," *Appl. Therm. Eng.*, vol. 28, no. 14–15, pp. 1782–1790, Oct. 2008, doi: 10.1016/j.applthermaleng.2007.11.011.
- [5] A. A. Al-abidi, S. Bin Mat, K. Sopian, M. Y. Sulaiman, and A. Th. Mohammed, "CFD applications for latent heat thermal energy storage: a review," *Renew. Sustain. Energy Rev.*, vol. 20, pp. 353–363, Apr. 2013, doi: 10.1016/j.rser.2012.11.079.
- [6] A. M. Soodmand et al., "A comprehensive review of computational fluid dynamics simulation studies in

phase change materials: applications, materials, and geometries,” *J. Therm. Anal. Calorim.*, Aug. 2023, doi: 10.1007/s10973-023-12438-0.

[7] “Multiphysics simulations: Challenges and opportunities - David E Keyes, Lois C McInnes, Carol Woodward, William Gropp, Eric Myra, Michael Pernice, John Bell, Jed Brown, Alain Clo, Jeffrey Connors, Emil Constantinescu, Don Estep, Kate Evans, Charbel Farhat, Ammar Hakim, Glenn Hammond, Glen Hansen, Judith Hill, Tobin Isaac, Xiangmin Jiao, Kirk Jordan, Dinesh Kaushik, Efthimios Kaxiras, Alice Koniges, Kihwan Lee, Aaron Lott, Qiming Lu, John Magerlein, Reed Maxwell, Michael McCourt, Miriam Mehl, Roger Pawlowski, Amanda P Randles, Daniel Reynolds, Beatrice Rivière, Ulrich Rüde, Tim Scheibe, John Shadid, Brendan Sheehan, Mark Shephard, Andrew Siegel, Barry Smith, Xianzhu Tang, Cian Wilson, Barbara Wohlmuth, 2013.” <https://journals.sagepub.com/doi/full/10.1177/1094342012468181> (accessed Sep. 13, 2023).

[8] M. Pater, B. Kaaks, B. Lauritzen, and D. Lathouwers, “A numerical benchmark for modelling phase change in molten salt reactors,” *Ann. Nucl. Energy*, vol. 194, p. 110093, Dec. 2023, doi: 10.1016/j.anucene.2023.110093.

[9] H.-J. Song and J.-W. Park, “Validation of Melting Computation Method for Reactor Vessel Ablation under External Reactor Vessel Cooling Conditions,” 2015.

[10] M. Torlak and A. Teskeredži, “MODELING AND SIMULATION OF HEAT STORAGE IN PHASE-CHANGE MATERIALS BASED ON COMPUTATIONAL FLUID DYNAMICS”.

[11] M. A. Dekhil, J. V. S. Tala, O. Bulliard-Sauret, and D. Bougeard, “Numerical analysis of the solidification process of water used as PCM in a rectangular latent heat thermal storage unit,” *J. Phys. Conf. Ser.*, vol. 2116, no. 1, p. 012044, Nov. 2021, doi: 10.1088/1742-6596/2116/1/012044.

[12] H. Gao, M. Chen, J. Hong, Y. Song, and Y. Yan, “Investigation on battery thermal management based on phase change energy storage technology,” *Heat Mass Transf.*, May 2021, doi: 10.1007/s00231-021-03061-6.